Bright near infrared neodymium emission from europium sensitisation in *β*-triketonate coordination polymers

Laura Abad Galán,[a,b] Alexandre N. Sobolev,[c] Brian W. Skelton,[c] Eli Zysman-Colman,[*b] Mark I. Ogden,[*a] and Massimiliano Massi[*a]

Isomorphous *β*-triketonate-based lanthanoid polymers containing tris(4-methylbenzoyl)methane (**mtbm**) and RbOH with formula, $\{[Ln(Rb)(\mathbf{mtbm})_4]_2\}_n$ (Ln = Eu^{3+} and Nd^{3+}) have been synthesised and structurally characterised. The photophysical properties for the Nd^{3+} complex presented long lifetimes and relatively high quantum yields in comparison with analogous *β*-diketonate complexes. Mixed lanthanoid complexes were also formed and their luminescence properties studied, with effective sensitisation of the $^4F_{3/2}$ of Nd^{3+} via the $^5D_0$ of Eu^{3+}, which is to the best of our knowledge the first example of Eu^{3+} to Nd^{3+} sensitisation in coordination polymers.

Introduction

Much attention has been paid to materials incorporating trivalent lanthanoid cations due to their unique photophysical properties such as their line-like emission spectra and their long-lived excited state lifetimes as a result of intraconfigurational *f-f* transitions. In addition, their emission colours range from the UV to the near infrared (NIR), dependant only on the metal cation. The NIR region is of particular interest due to potential applications in a wide range of fields including optical displays, night vision devices, telecommunication signalling and life science.[1–6] However, trivalent lanthanoid cations cannot be directly excited as intra-*f* transitions are parity, and often spin, forbidden. Therefore, π-conjugated ligands are often used as sensitisers because of their greater capacity to absorb light. This efficient pathway is well established and normally occurs by energy transfer from the triplet state of the ligand, being previously populated via intersystem crossing, to the excited energy level of the lanthanoid.[7,8] However, there are other possible pathways to sensitise lanthanoid emission, such as via *d*-metals[9–12] or other lanthanoids.[13–20] Furthermore, the excited state of NIR-emitting lanthanoids can easily be quenched by multiphonon relaxation with high energy oscillators such as OH, NH or CH.[7]

β-Diketones have commonly been used as antenna ligands because of their good chelating properties and their ability to effectively sensitise the trivalent lanthanoid excited states. In fact, a variety of *β*-diketones Nd^{3+} complexes can be found in the literature in the last couple of decades.[21–28] However, reported quantitative data (quantum yields, lifetimes) are very limited. The design of the *β*-diketonate Nd^{3+} complexes typically involves two main strategies: lowering the triplet state of the antenna in order to favour the energy transfer to Nd^{3+} and minimising the nonradiative relaxation pathways. [24,25]

We have previously reported that *β*–triketonate ligands can efficiently transfer energy to the *4f** states, showing exceptional photophysical properties for the NIR emitters, Yb^{3+} and Er^{3+} in particular.[29] Our previous studies with tris(4-methylbenzoyl)methane (**mtbm**) resulted in the isolation and characterisation of polymeric structures of formulation $\{[Ln(Cs)(\mathbf{mtbm})_4]_2\}_n$ (Ln^{3+} = Eu and Er) and $[Yb(CsHOEt)(\mathbf{mtbm})_4]_n$.[30] This contrasted with the discrete tetranuclear Ae_2Ln_2 assemblies formed with tribenzoylmethane (**tbm**).[25]

In this work, we extend the study to Nd^{3+} complexes, presenting the synthesis and crystal structures of the resulting assemblies. The photophysical properties of the assemblies have been studied via two different sensitisation pathways: energy transfer from the triplet state of the ligand, and from the $^5D_0$ of Eu^{3+}. While energy transfer between Eu^{3+} and Nd^3 has been extensively studied in doped glasses[32–36], only one discrete complex showing Eu/Nd energy migration has previously been reported.[37] The work presented herein is, to the best of our knowledge, the first example of a coordination polymer containing Eu/Nd ions, with effective lanthanoid-lanthanoid sensitisation from the $^5D_0$ of Eu^{3+} to the 4*f** of Nd^{3+}.

Experimental

General procedures

All reagents and solvents were purchased from chemical suppliers and used as received without further purification. The ligand tribenzoylmethane (**tbm**H), was prepared as previously reported.[31] Hydrated $LnCl_3$ (Ln = Eu^{3+}, Er^{3+}, Yb^{3+}) was prepared by the reaction of Ln_2O_3 with hydrochloric acid (5 M), followed

[a] *Department of Chemistry, and Curtin Institute for Functional Molecules and Interfaces, Curtin University, Kent Street, Bentley 6102 WA, Australia.*
[b] *Organic Semiconductor Centre, EaStCHEM School of Chemistry, University of St. Andrews, St. Andrews, Fife, KY16 9ST, United Kingdom*
[c] *School of Molecular Sciences, M310, University of Western Australia, Crawley 6009 WA, Australia.*
*E-mail: m.massi@curtin.edu.au; m.ogden@curtin.edu.au; eli.zysman-colman@st-andrews.ac.uk
† Electronic Supplementary Information (ESI) available:

by evaporation of the solvent under reduced pressure. Infrared spectra (IR) were recorded on solid-state samples using an attenuated total reflectance Perkin Elmer Spectrum 100 FT-IR. IR spectra were recorded from 4000 to 650 cm^{-1}; the intensities of the IR bands are reported as strong (s), medium (m), or weak (w), with broad (br) bands also specified. Melting points were determined using a BI Barnsted Electrothermal 9100 apparatus. Elemental analyses were obtained at Curtin University, Australia. Nuclear magnetic resonance (NMR) spectra were recorded using a Bruker Avance 400 spectrometer (400.1 MHz for ^{1}H; 100 MHz for ^{13}C) at 300 K. The data were acquired and processed by the Bruker TopSpin 3.1 software. All of the NMR spectra were calibrated to residual solvent signals.

Selected Equations

The values of the radiative lifetime (τ_R), and intrinsic quantum yield (Φ^{Ln}_{Ln}), can be calculated with the following equations.[36]

$$\frac{1}{\tau_R} = 14.65\,s^{-1} \times n^3 \times \frac{I_{Tot}}{I_{MD}} \quad (eq.\ 1)$$

In equation 1, the refractive index (n) of the solvent is used (assumed value of 1.5 in the solid state), the value 14.65 s^{-1} is the spontaneous emission probability of the $^7F_1 \leftarrow {}^5D_0$ transition reported previously. I_{Tot} is the total integration of the Eu^{3+} emission spectrum, and I_{MD} is the integration of the $^7F_1 \leftarrow {}^5D_0$ transition.

$$\Phi^{Ln}_{Ln} = \frac{\tau_{obs}}{\tau_R} \quad (eq.\ 2)$$

The sensitization efficiency (η_{sens}) can be determined using equation 3 below:

$$\eta_{sens} = \frac{\Phi^{L}_{Ln}}{\Phi^{Ln}_{Ln}} \quad (eq.\ 3)$$

The rate of energy transfer (K_{ET}) and quantum efficiency of energy transfer (Φ_{ET}) can be calculated according to the following equations:

$$K_{ET} = \frac{1}{\tau_q} - \frac{1}{\tau_u} \quad (eq.4)$$

$$\Phi_{ET} = 1 - \frac{\tau_q}{\tau_u} \quad (eq.5)$$

In equations 4-5, τ_q and τ_u are the ^5D_o decay lifetime of Eu^{3+} in the presence or absence of the quencher (Nd^{3+}), respectively.

For dipole-dipole exchange mechanisms or Forster the donor-acceptor distance (R_{DA}) can be calculated following equation 6:

$$\Phi_{FRET} = \frac{1}{1+\left(\frac{R_{DA}}{R_0}\right)^6} \quad (eq.\ 6)$$

Where R_0 is the critical distance for a 50% transfer, being tabulated to be 9.05 Å for the Eu^{3+}-Nd^{3+} pair.[38]

Photophysical Measurements

Absorption spectra were recorded at room temperature using a Perkin Elmer Lambda 35 UV/Vis spectrometer. Uncorrected steady-state emission and excitation spectra were recorded using an Edinburgh FLSP980-stm spectrometer equipped with a 450 W xenon arc lamp, double excitation and emission monochromators, a Peltier-cooled Hamamatsu R928P photomultiplier (185–850 nm) and a Hamamatsu R5509-42 photomultiplier for detection of NIR radiation (800-1400 nm). Emission and excitation spectra were corrected for source intensity (lamp and grating) and emission spectral response (detector and grating) by a calibration curve supplied with the instrument. Overall quantum yields (Φ^{L}_{Ln}) were measured with the use of an integrating sphere coated with BenFlect.[39] In the case of the NIR, overall quantum yields were measured using two different detectors and [Yb(phen)(tta)$_3$] ($\Phi^{L}_{Ln} = 1.6\%$)[40], where tta is thenoyltrifluoroacetone, as reference to calibrate the set up according to the procedure previously reported by our group.[41]

Excited-state decays (τ) were recorded on the same Edinburgh FLSP980-stm spectrometer using a microsecond flashlamp. The goodness of fit was assessed by minimizing the reduced χ^2 function and by visual inspection of the weighted residuals.

Synthesis

Di(4-methylbenzoyl)methane (mdbmH)

The **mdbm**H precursor was synthesized following a previously reported procedure.[30]

Lanthanoid assemblies

RbOH (4 eq) was added to a mixture containing **mtbm**H; (4 eq) and hydrated $LnCl_3$ (ca. 20 mg) in ethanol (10 mL). The mixture was heated at reflux for 30 minutes and filtered over a glass frit while still hot. The filtered solution was then left undisturbed at ambient temperature and slow evaporation of the solvent over several days afforded crystals suitable for X-ray diffraction.

{[Eu(Rb)(**mtbm**)$_4$]$_2$}$_n$: M.p. 267-269 °C. Elemental analysis calcd (%) for $C_{200}H_{168}Rb_2Eu_2O_{24}$ (1.75·H_2O): C, 68.53; H, 5.05; found: C, 68.53; H, 4.74. IR (ATR): ν = 2919 w, 1634 w, 1602 m, 1577 m, 1538 s, 1408 m, 1360 s, 1275 m, 1183 m, 1151 m, 1115 w, 1021 w, 899 s, 837 m, 7836 s, 721 m, 694 w.

{[Nd(Rb)(**mtbm**)$_4$]$_2$}$_n$: M.p. 289-291 °C. Elemental analysis calcd (%) for $C_{100}H_{84}RbNdO_{12}$ (1.5·$H_2$0): C, 66.49; H, 5.30; found: C, 66.24; H, 4.93. IR (ATR): ν = 2920 w, 2164 w, 1634 m, 1602 m, 1574 m, 1529 s, 1405 m, 1342 s, 1273 m, 1184 m, 1151 m, 1112 w, 1034 w, 899 s, 825 m, 780 s, 763 s, 721 m.

[Nd(Rb·HOEt)(**tbm**)$_4$]$_2$: M.p. 259-261 °C. Elemental analysis calcd (%) for $C_{180}H_{132}Rb_2Nd_2O_{26}$: C, 68.19; H, 4.20; found: C, 67.70; H, 3.78. IR (ATR): ν = 3065 w, 1739 w, 1644 w, 1645w, 1597 w, 1583 m, 1540 m, 1491 w, 1448 m, 1374 s, 1297 s, 1277 s, 1181 w, 1151 m, 1073 w, 1012 w, 897 s, 823 m, 779 w, 747 s.

Crystallography

Crystallographic data for the structures were collected at 100(2) K on an Oxford Diffraction Gemini or Xcalibur diffractometer using Mo Kα or Cu Kα radiation**.** Following absorption corrections and solution by direct methods, the structures were refined against F^2 with full-matrix least-squares using the program SHELX-2014.[39]

Unless stated below, anisotropic displacement parameters were employed for the non-hydrogen atoms. All hydrogen atoms were added at calculated positions and refined by use of a riding model with isotropic displacement parameters based on those of the parent atom. CCDC deposits contain supplementary crystallographic data, and can be obtained free of charge *via* http://www.ccdc.cam.ac.uk/conts/retrieving.html, or from the Cambridge Crystallographic Data Centre, 12 Union Road, Cambridge CB2 1EZ, U.K.; fax: (+44) 1223-336-033; or e-mail: deposit@ccdc.cam.ac.uk

{[Eu(Rb)(**mtbm**)$_4$]$_2$}$_n$: $C_{200}H_{168}Eu_2O_{24}Rb_2 \cdot (H_2O)$, M = 3448.20, crystal size 0.23 x 0.07 x 0.05 mm^3, triclinic, space group $P\bar{1}$ (No. 2), a = 14.9383(5), b = 15.9699(4), c = 17.9990(7) Å, α = 84.625(2),β = 74.799(3), γ = 88.086(2)°, V = 4125.3(2) Å^3, Z = 1, D_c = 1.388 g/cm^3, μ = 6.673 mm^{-1}. F_{000} = 1770, Cu Kα radiation, λ = 1.54178 Å, $2\theta_{max}$ = 134.8°, 44958 reflections collected, 14682 unique (R_{int} = 0.0549). Final *GooF* = 1.059, *R1* = 0.0386, *wR2* = 0.0890, *R* indices based on 13164 reflections with $I > 2\sigma(I)$, $|\Delta\rho|_{max}$ = 0.67 e Å^{-3}, 1054 parameters, 3 restraints. The water molecule hydrogen atoms were refined with geometries restrained to ideal values. CCDC 1829212.

{[Nd(Rb)(**mtbm**)$_4$]$_2$}$_n$: $C_{200}H_{168}Nd_2O_{24}Rb_2 \cdot (H_2O)$, M = 3432.77, crystal size 0.167 x 0.044 x 0.028 mm^3, triclinic, space group $P\bar{1}$ (No. 2), a = 14.9907(3), b = 15.9632(3), c = 17.9930(4) Å, α = 84.954(2), β = 74.674(2), γ = 88.124(2)°, V = 4136.30(15) Å^3, Z = 1, D_c = 1.378 g cm^{-3}, μ = 6.017 mm^{-1}. F_{000} = 1764, Cu Kα radiation, λ = 1.54178 Å, $2\theta_{max}$ = 134.6°, 89010 reflections collected, 14738 unique (R_{int} = 0.0665). Final *GooF* = 1.001, *R*1 = 0.0335, *wR*2 = 0.0787, *R* indices based on 13047 reflections with $I > 2\sigma(I)$, $|\Delta\rho|_{max}$ = 0.84 e Å^{-3}, 1054 parameters, 9 restraints. The water molecule hydrogen atoms were refined with geometries restrained to ideal values. CCDC 1829213.

[Nd(Rb·HOEt)(**tbm**)$_4$]$_2$: $C_{180}H_{132}Nd_2O_{26}Rb_2 \cdot 2(C_2H_6O)$, M = 3262.40, crystal size 0.31 x 0.21 x 0.12 mm^3, triclinic, space group $P\bar{1}$ (No. 2), a = 14.0539(2), b = 14.7835(3), c = 19.7708(4) Å, α = 99.829(2), β = 107.431(2), γ = 90.137(2)°, V = 3855.27(13) Å^3, Z = 1, D_c = 1.405 g/cm^3, μ = 1.367 mm^{-1}. F_{000} = 1666, Mo Kα radiation, λ = 0.71073 Å, $2\theta_{max}$ = 64.7°, 84599 reflections collected, 25545 unique (R_{int} = 0.0650). Final *GooF* = 1.002, *R1* = 0.0496, *wR2* = 0.0959, *R* indices based on 19518 reflections with $I > 2\sigma(I)$, $|\Delta\rho|_{max}$ = 1.1 e Å^{-3}, 961 parameters, 13 restraints. One phenyl ring and two solvent ethanol molecules were modelled as being disordered over two sets of sites with occupancies constrained to 0.5 and with the non-hydrogen atoms refined with isotropic displacement parameters. Geometries of the disordered atoms were restrained to ideal values. CCDC 1829214.

[Yb(**mtbm**)$_3$(OH$_2$)]$_2$: $C_{75}H_{65}O_{10}Yb \cdot 0.5(C_2H_6O)$, M = 1322.34, crystal size 0.31 x 0.042 x 0.038 mm^3, monoclinic, space group $P2_1/n$, a = 10.5065(12), b = 22.8219(3), c = 26.2567(3) Å, β = 90.116(2)°, V = 6295.8(7) Å^3, Z = 4, D_c = 1.395 g/cm^3, μ = 3.245 mm^{-1}. F_{000} = 2712, Cu Kα radiation, λ = 1.54178 Å, $2\theta_{max}$ = 134.9°, 66086 reflections collected, 11254 unique (R_{int} = 0.0839). Final *GooF* = 1.069, *R1* = 0.0486, *wR2* = 0.1117, *R* indices based on 8726 reflections with $I > 2\sigma(I)$, $|\Delta\rho|_{max}$ = 1.7 e Å^{-3}, 820 parameters, 17 restraints. The solvent was modelled as an ethanol molecule disordered about a crystallographic inversion centre. Geometries were restrained to ideal values. Water molecule hydrogen atoms were located and refined with geometries restrained to ideal values. CCDC 1829215.

*[Nd(Cs·2HOEt)(**dbm**)$_4$]$_n$:* $C_{64}H_{56}CsNdO_{10}$, M = 1262.23, crystal size 0.26 x 0.084 x 0.053 mm^3, monoclinic, space group *C*2/*c*, *a* = 27.4726(6), *b* = 8.29060(10), *c* = 25.4388(6) Å, β = 108.315(2)°, V =5500.5(2) Å^3, Z = 4, D_c = 1.524 g/cm^3, μ = 12.772 mm^{-1}. F_{000} =2540, Cu Kα radiation, λ = 1.54178 Å, $2\theta_{max}$ = 134.6°, 29516 reflections collected, 4906 unique (R_{int} = 0.0436). Final *GooF* = 1.090, *R1* = 0.0386, *wR2* = 0.1095, *R* indices based on 4314 reflections with $I > 2\sigma(I)$, $|\Delta\rho|_{max}$ = 2.5 e Å^{-3}, 349 parameters, 0 restraints. CCDC 1829216.

*[Cs(**mtbm**)]$_n$:* $C_{25}H_{21}CsO_3$, M = 502.33, crystal size 0.240 x 0.057 x 0.042 mm^3, monoclinic, space group $P2_1/c$, a = 8.41028(14), b = 31.2556(4), c = 8.01519(14) Å, β = 102.777(2)°, V = 2054.77(6) Å^3, Z = 4, D_c = 1.624 g/cm^3, μ = 14.245 mm^{-1}. F_{000} =1000, Cu Kα radiation, λ = 1.54178 Å, $2\theta_{max}$ = 134.6°, 17616 reflections collected, 3671 unique (R_{int} = 0.0558). Final *GooF* = 1.037, *R1* = 0.0455, *wR2* = 0.1174, *R* indices based on 3361 reflections with $I > 2\sigma(I)$, $|\Delta\rho|_{max}$ = 2.4 e Å^{-3}, 265 parameters, 0 restraints. CCDC 1829217.

Results and discussion

The **tbm**H and **mtbm**H molecules were synthesised according to the previously reported methodology. [30,42] Following a similar procedure to that previously reported for the preparation of {[Ln(Cs)(**tbm**)$_4$]$_2$} (Ln^{3+}= Eu, Er, Yb) and {[Ln(Cs)(**mtbm**)$_4$]$_2$}$_n$ (Ln^{3+}= Eu, Er),[30] one equivalent of hydrated $LnCl_3$ (Ln^{3+}= Eu, Nd) was made to react with four equivalents of **mtbm**H and four equivalents of RbOH in ethanol. Slow evaporation of the solvent resulted in the formation of suitable crystals for X-Ray diffraction revealing the formation of coordination polymers with formula {[Ln(Rb)(**mtbm**)$_4$]$_2$}$_n$ where Ln^{3+}= Eu(**1**), Nd(**2**). The compositions of the isolated species were further confirmed by elemental analysis and IR spectroscopy.

The Eu^{3+}/Nd^{3+} mixed assemblies were synthesised in a similar fashion to the $\{[Ln(Rb)(\mathbf{mtbm})_4]_2\}_n$ except for the use of mixtures of hydrated $EuCl_3$ and $NdCl_3$ in molar ratios of Nd^{3+} of 0.25(**3**), 0.50(**4**) and 0.75(**5**).

Analogous studies were attempted with CsOH and $NdCl_3$ in order to assess the effect of the different alkaline base in the mixed systems; however only the cesium-containing coordination polymer $[Cs(\mathbf{mtbm})]_n$ was deposited (see supplementary information). [30]

When the same procedure was followed for the hydrated $NdCl_3$ and **tbm**H with RbOH or CsOH, the formation of assemblies with formula $[Nd(Rb)(\mathbf{tbm})_4]_2$ and $[Nd(Cs{\cdot}2HOEt)(\mathbf{dbm})_4]_n$ were found, respectively. The $[Nd(Rb)(\mathbf{tbm})_4]_2$ (**6**) complex presents a similar structure to the previously reported tetranuclear assemblies.[31] In contrast, the isolation of the $[Nd(Cs{\cdot}2HOEt)(\mathbf{dbm})_4]_n$ linear polymer shows the second example of a possible *in situ* retro-Claisen condensation reaction of **tbm**H in the presence of CsOH and hydrated $NdCl_3$ resulting in the formation of a *β*-diketonate complex similar to previously reported examples (see supplementary information).[30] The hypothesis that the triketonate ligands undergo a retro-Claisen condensation reaction under these reaction conditions is currently under investigation and the results will be presented elsewhere.

Finally, when the same procedure was attempted with $YbCl_3$, a dimeric structure was crystallised with formula $[Yb(\mathbf{mtbm})_3(H_2O)_2]_2$ (see supplementary information). Due to difference in composition and symmetry of this structure in comparison with the polymeric species of complexes **1** and **2**, Yb^{3+} was not further investigated for the purpose of this study.

X-ray diffraction

Table 1. Selected bond lengths and intermetallic distances (Å) for complexes **1**, **2** and **6**.

	1 $\{[\mathbf{Eu}(Rb)(mtbm)_4]_2\}_n$	**2** $[\mathbf{Nd}(Rb)(mtbm)_4]_2\}_n$	**6** $[\mathbf{Nd}(Rb{\cdot}HOEt)(tbm)_4]_2$
Ln-O	2.327(2)-2.405(2)	2.363(2)-2.444(2)	2.390(2)-2.450(2)
Ae-O	2.816(2)-2.983(2)	2.817(2)-2.989(2)	2.822(2)-3.051(2)
Ae(1)-Ae(2)	8.1196(5)	8.1312(5)	8.3053(6)
Ae(1)-Ae(2')	8.7992(5)	8.8013(5)	-
Ln(1)-Ln(2)	9.4915(5)	9.5391(5)	8.9836(5)
Ln(1)-Ln(2')	11.0901(6)	11.0929(5)	13.8915(6)
Ln(1)-Ae(1)	4.0943(4)	4.1044(3)	4.1340(3)
Ln(1)-Ae(2)	8.1849(5)	8.8169(5)	7.5993(6)
Ae(2)-Ln(1')	8.8145(5)	8.2087(5)	-
Ln(1)-Ln(1*)	14.9383(7)	14.9907(5)	14.0539(5)

'subsequent units and * different chain

The structures of the two $\{[Ln(Rb)(\mathbf{mtbm})_4]_2\}_n$ (Ln^{3+}= Nd, Eu) complexes are isomorphous and structurally similar to the Cs-based polymers with formula $\{[Ln(Cs)(mtbm)_4]_2\}_n$ (Ln^{3+}= Eu,Er).[30] The units formed of two Ln^{3+}, two Rb^+ metal centres and eight **mtbm**$^-$ ligands are isomorphous to the previously reported tetranuclear assemblies.[29] The Ln^{3+} is eight coordinated, with four **mtbm**$^-$ ligands coordinated by two of the 0-keto atoms in a bidentate mode. In this case, the third O-keto of two of the ligands are linked to Rb^+ cations forming the tetranuclear assembly and the polymer, respectively (Figure 1).

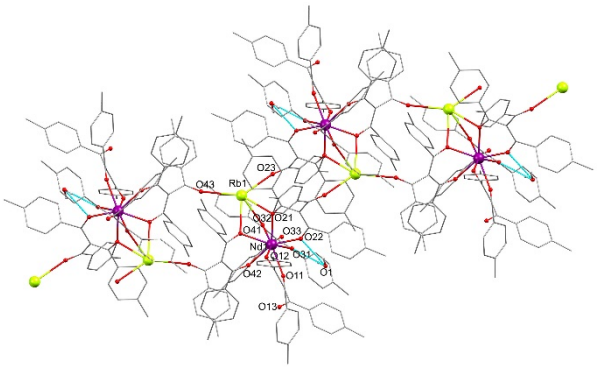

Figure 1 Representation of the X-Ray structure of **2**, $\{[Nd(Rb)(\mathbf{mtbm})_4]_2\}_n$, where hydrogens have been omitted for clarity.

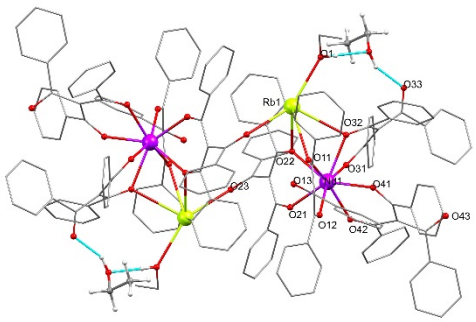

Figure 2 Representation of the X-Ray structure of **6**, $[Nd(Rb)(\mathbf{tbm})_4]_2$, where hydrogens have been omitted for clarity except for those on the solvent EtOH molecule.

Table 2 Photophysical data for the complexes in the solid state

Complex	X^{a}_{Nd3+}	λ_{exc}(nm)	λ_{em}(nm)	τ_{obs}(μs)	τ_r(ms)	Φ^{Ln}_{Ln}(%)	Φ^{L}_{Ln}(%)[b]	χ	K_{ET}(s^{-1})	τ_{ET}(s)	Φ_{ET}(%)
1	0	350	612	507	0.86	59	31	52	-	-	-
2	1	350	1060	11	0.27[c]	4.2	1.34	32	-	-	-
		350	612	335	0.681	49	17.5	35			
3	0.25	350	1060	8.7	0.27[c]	3.1	0.23	7	$1.0\cdot10^{3}$	$9.87\cdot10^{-4}$	34
		350	612	183	0.46	40	6.55	16			
4	0.5	350	1060	11.0	0.27[c]	4.1	0.74	18	$3.5\cdot10^{3}$	$2.86\cdot10^{-4}$	64
		350	612	143	0.54	27	1.44	5			
5	0.75	350	1060	8.7	0.27[c]	3.2	0.44	14	$5.0\cdot10^{3}$	$1.99\cdot10^{-4}$	72
6	1	350	1060	8.8	0.27[c]	3.3	0.58	17	-	-	-

[a] solution phase compositions in the reaction mixture [b] quantum yield measured with the use of an integrating sphere [c] literature value for Nd^{3+}[27]

Here, a H_2O molecule is found in the lattice with two hydrogen bonds formed with two keto O(22) and O(31). Intermolecular interactions between chains are present where the lanthanoid centres sit at distances longer than 14Å (see supplementary nformation). The geometry of the eight coordinate Ln^{3+} is best described as triangular dodecahedron (see supplementary information).

The structure of the [Nd(Rb·HOEt)(**tbm**)$_4$]$_2$ is isomorphous to the previously published tetranuclear assemblies where the eight coordinated Nd^{3+} adopts a geometry best described as distorted triangular dodecahedron (Figure 2).

Photophysical investigation

The photophysical data for complexes **1**-**6** including excited state lifetime decay (τ_{obs}), calculated radiative decay (τ_R), intrinsic photoluminescence quantum yield (Φ_{Ln}^{Ln}), overall photoluminescence quantum yield (Φ_{Ln}^{L}), and calculated sensitisation efficiency (η_{sens}), are reported in Table 2. The emission properties were recorded in the solid state due to the low stability of the complexes in polar solvents and poor solubility in nonpolar solvents as previously demonstrated.[29]
As shown before, the energy of the **mtbm** and **tbm** triplet states (21,140 cm^{-1} and 20,704 cm^{-1})[29,30] are sufficiently high to sensitise the $^5D_0$ (~17,200 cm^{-1}) of Eu^3, the $^2F_{5/2}$ (~10,200 cm^{-1}) of Yb^{3+} and the $^4I_{13/2}$ (~6,566 cm^{-1}) of Er^{3+}. Therefore, energy transfer to the $^4F_{3/2}$ (~11,260 cm^{-1}) state of Nd^{3+} is also expected. In fact, each emission spectrum shown herein is the result of an effective antenna effect supported by the broad excitation spectra which matches with the absorption profile of the corresponding ligands.

The emission spectrum of {[Eu(Rb)(**mtbm**)$_4$]$_2$}$_n$ (**1**) shows the characteristic Eu^{3+} emission bands attributed to the $^7F_J \leftarrow {}^5D_0$ (J= 0-6) region 580-820 nm (Figure 3). The $^7F_0 \leftarrow {}^5D_0$ transition is strictly forbidden by the selection rules and is only observable for low symmetry complexes. The lack of this band in our system suggests a higher symmetry than C_{nv}, C_n or C_s. The magnetic dipole-allowed band ($^7F_1 \leftarrow {}^5D_0$) is split into two sublevels inherent to tetragonal crystal fields. This is in agreement with the splitting of the hypersensitive band ($^7F_2 \leftarrow {}^5D_0$) in four sublevels. The splitting of the main transitions is in accordance with the shape analysis which suggests that the local symmetry of the Eu^{3+} cation is best described as a distorted triangular dodecahedron.

Excited state decay was fitted to a monoexponential function giving a value of observable lifetime (τ_{obs}) of 507 μs. From the emission spectrum, the radiative decay (τ_r) was calculated to be 0.86 ms. With an integrating sphere, the overall quantum yield (Φ^{L}_{Ln}) was measured as 31%. From these data, the intrinsic quantum yield (Φ^{Ln}_{Ln}) as ratio τ_{obs} /τ_r could be calculated to be 59% with a sensitization efficiency of 52%.

These data are of the same order as the previously reported {[Eu(Cs)(**mtbm**)$_4$]$_2$}$_{n,}$[30] showing that the exchange in the alkaline base has little impact on the photophysical properties.

The emission spectrum of {[Nd(Rb)(**mtbm**)$_4$]$_2$}$_n$ (**2**) shows the characteristic Nd^{3+} emission bands from the $^7I_J \leftarrow {}^4F_{3/2}$ (J= 9/2, 11/2, 13/2) with maxima at 910, 1060 and 1350 nm respectively

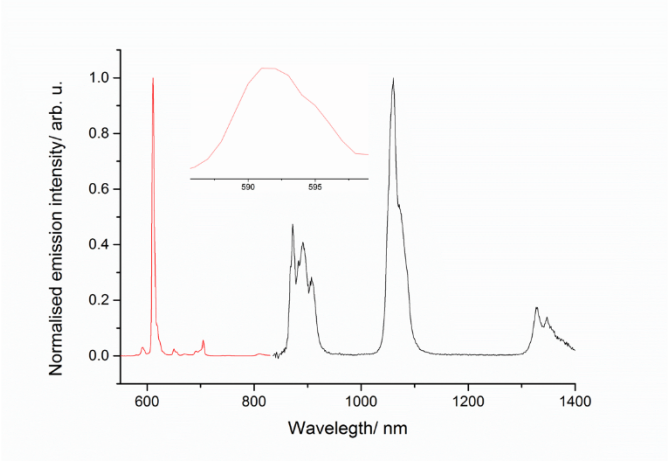

Figure 3 Normalised emission plot for $\{[Eu(Rb)(\mathbf{mtbm})_4]_2\}_n$ (red trace) and $\{[Nd(Rb)(\mathbf{mtbm})_4]_2\}_n$ (black trace) in the solid state, with excitation wavelength at 350nm. Inset: highlight of the splitting of the magnetic dipole transition for the Eu^{3+} complex.

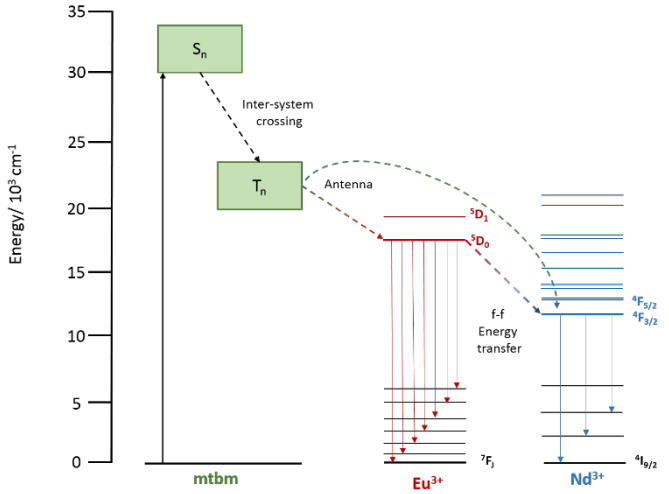

Figure 4 Energy level diagram and energy transfer occurring for the mixed complexes $\{[Eu_{1-x}Nd_x(Rb)(\mathbf{mtbm})_4]_2\}_n$

(Figure 3). These bands are structured as a consequence of the crystal field effect from the ligands. The excited state decay was measured to be 11 µs after deconvolution from instrumental response. This value of τ_{obs} is relatively high in comparison to the previously reported *β*-diketonate compounds[21,28] and of the same order of magnitude as highly conjugated systems.[25,44]

Although it is known that the radiative decay for Nd^{3+} ranges from 0.2 to 0.5 ms[4], a standard value of 0.27 ms[27] is generally accepted for the Nd^{3+} complexes in the solid state. The intrinsic quantum yield can therefore be estimated to 4.2%. The overall quantum yield using an integrating sphere following previously reported procedure for the use of two different detectors[41] was found to be 1.34%, with a sensitization efficiency of 32%. These data suggest that reducing non-radiative decays due to the removal of the C-H bond is an effective way to enhance the photophysical properties of the Nd^{3+} emitters.

As the structures for Eu^{3+} and Nd^{3+} are isomorphous, $\{[Ln(Rb)(\mathbf{mtbm})_4]_2\}_n$, mixtures of both lanthanoids were prepared (**3**-**5**) in order to investigate sensitisation of the $^4F_{3/2}$ of Nd^{3+} via the $^5D_0$ of Eu^{3+} (Figure 4).

The emission spectra of the mixed complexes show the characteristic emission bands from the $^7F_J \leftarrow {}^5D_0$ (J= 0-6) of Eu^{3+} in the visible region (580-820 nm) and the $^7I_J \leftarrow {}^4F_{3/2}$ (J= 9/2, 11/2, 13/2) Nd^{3+} bands in the NIR region (850 -1400 nm) with identical splitting in comparison with the pure complexes **1** and **2**, respectively. This suggests that the structure is preserved with the mixed lanthanoid polymers. The intensity of the Nd^{3+} emission bands increases when the molar ratio of Nd^{3+} is higher (Figure 5). The lifetime of the excited state of Eu^{3+} is shortened as the amount of Nd^{3+} increases, from 507 µs for **1** to 335 µs, 183 µs and 143 µs for **3**, **4** and **5**, respectively. From these numbers, the highest energy transfer quantum efficiency can be calculated to be 72% for complex **5**. Overall quantum yields were measured, finding decreasing values for Eu^{3+} of 17.5%, 6.55% and 1.44% for complexes **3**-**5**, respectively, while the values for Nd^{3+} remain constant (see table 2). The sensitisation efficiency for Nd^{3+} for the mixed complexes is slightly lower than in the pure complex **2** where the only pathway of energy transfer is via the antenna effect.

This is probably due to long Ln···Ln distances. Typically, energy transfer between lanthanoid centres is considered limited for distances longer than 9Å due to slow energy migration.[45] In fact, if a purely dipole-dipole exchange mechanism is considered, the donor- acceptor distance can be calculated to be 7.7Å following equation 6, for a quantum efficiency of energy transfer (Φ_{ET}) of 0.72 for complex **5**. However in our system, the shortest distance between two lanthanide centres is 9.5 Å. Therefore, the sensitisation to **f* states of Nd^{3+} from the $^5D_0$ of Eu^{3+} for complexes **3**-**5** may be ligand mediated.[46,47]

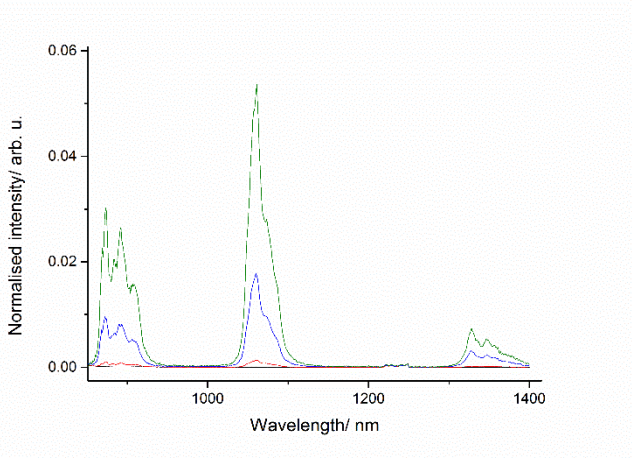

Figure 5 Nd^{3+} emission plot for complex **2** (black trace), **3** (red trace), **4** (blue trace) and **5** (green trace) with excitation wavelength at 350nm.

For control experiments, equimolar mechanically-ground mixtures of **1** and **2** were studied**.** The lifetime of the $^5D_0$ of Eu^{3+} was found to be 356 μs, suggesting that there is energy transfer between chains that may occur via intermolecular interactions (see supplementary information).

Finally, the emission spectrum of $[Nd(Rb{\cdot}HOEt)(\mathbf{tbm})_4]_2$ (**6**) shows the three characteristic Nd^{3+} bands from the $^7I_J \leftarrow {}^4F_{3/2}$ (J= 9/2, 11/2, 13/2) similarly to the $\{[Nd(Rb)(\mathbf{mtbm})_4]_2\}_n$ (**1**) (see supplementary information). The values of lifetime (τ_{obs}), intrinsic quantum yield (Φ^{Ln}_{Ln}) and overall quantum yield (Φ^{L}_{Ln}) were found to be 8.85 μs, 3.3% and 0.58%, respectively. The main difference with complex 2 arises from a lower overall quantum yield, maintaining the values of lifetime and intrinsic quantum yields, which suggests that the sensitisation process from **tbm** to the 4*f** accepting states of Nd^{3+} is not as efficient as in the **mtbm** based complexes.

Conclusions

In this report the study of *β*-triketonate based lanthanoid complexes has been extended to Nd^{3+}, presenting new examples of tetranuclear assemblies ($[Nd(Rb{\cdot}HOEt)(\mathbf{tbm})_4]_2$) and coordination polymers with formula $\{[Nd(Rb)(\mathbf{mtbm})_4]_2\}_n$. The fact that isomorphous structures were found for the **mtbm** and Eu^{3+} ($\{[Nd(Rb)(\mathbf{mtbm})_4]_2\}_n$), opened up the possibility to synthesise mixed lanthanoid complexes with the aim of achieving *f-f* energy transfer. Indeed, an example of a mixed **mtbm** based lanthanoid coordination polymer with efficient sensitisation from the $^5D_0$ of Eu^{3+} to the $^4F_{3/2}$ of Nd^{3+} was formulated. The emission studies of the pure and mixed complexes show particularly good photophysical properties in the case of Nd^{3+} via both mechanisms; standard antenna and *f-f* sensitisation.

Conflicts of interest

There are no conflicts to declare.

Acknowledgements

This research was partially supported by the Australian Research Council's Discovery *Projects* funding scheme (project DP17010189), and a Royal International Exchanges Grant. E.Z.-C. thanks the EPSRC (EP/M02105X/1) for support. M.M. wishes to thank the ARC for funding (FT1301000033). L.A.G thanks Curtin University for the Australian Postgraduate Award and the University of Montreal (UdeM). The authors acknowledge access to the facilities at the Centre for Microscopy, Characterisation and Analysis, University of Western Australia.

Notes and references

1 S. V. Eliseeva and J.-C. G. Bünzli, *Chem. Soc. Rev.*, 2010, **39**, 189–227.
2 J.-C. G. Bünzli, *Lumin. Lanthan. Ions Coord. Compd. Nanomater.*, 2014, **1st**, 125–196.
3 J.-C. G. Bünzli and S. V. Eliseeva, *J. Rare Earths*, 2010, **28**, 824–842.
4 J. C. G. Bünzli and S. V. Eliseeva, *Photophysics of Lanthanoid Coordination Compounds*, 2013, vol. 8.
5 V. V. Utochnikova, A. Grishko, A. Vashchenko, A. Goloveshkin, A. Averin and N. Kuzmina, *Eur. J. Inorg. Chem.*, 2017, 1–6.
6 S. V. Eliseeva and J.-C. G. Bünzli, *New J. Chem.*, 2011, **35**, 1165.
7 J. G. Bunzli and S. V Eliseeva, *Springer Ser. Fluoresc.*, 2011, 1–45.
8 S. Cotton, *Lanthanide and Actinide Chemistry*, 2005.
9 M. Mehlstäubl, G. S. Kottas, S. Colella and L. De Cola, *Dalt. Trans.*, 2008, **2**, 2385.
10 D. Sykes, A. J. Cankut, N. M. Ali, A. Stephenson, S. J. P. Spall, S. C. Parker, J. a Weinstein and M. D. Ward, *Dalton Trans.*, 2014, **43**, 6414–28.
11 A. Baschieri, S. Muzzioli, E. Matteucci, S. Stagni, M. Massi and L. Sambri, *Dalton Trans.*, 2015, **44**, 37–40.
12 W. S. Perry, S. J. A. Pope, C. Allain, B. J. Coe, A. M. Kenwright and S. Faulkner, *Dalt. Trans.*, 2010, **39**, 10974.
13 N. M. Shavaleev, S. J. A. Pope, Z. R. Bell, S. Faulkner and M. D. Ward, *Dalt. Trans.*, 2003, 808–814.
14 X. Rao, T. Song, J. Gao, Y. Cui, Y. Yang, C. Wu, B. Chen and G. Qian, *J. Am. Chem. Soc.*, 2013, **135**, 15559–64.
15 L. Song, Q. Wang, D. Tang, X. Liu and Z. Zhen, *New J. Chem.*, 2007, **31**, 506–511.
16 C. M. Andolina and J. R. Morrow, *Eur. J. Inorg. Chem.*, 2011, 154–164.
17 J. J. Lessmann and W. D. W. Horrocks, *Inorg. Chem.*, 2000, **39**, 3114–3124.
18 S. Faulkner and S. J. A. Pope, *J. Am. Chem. Soc.*, 2003, **125**, 10526–10527.
19 D. T. De Lill, A. De Bettencourt-Dias and C. L. Cahill, *Inorg. Chem.*, 2007, **46**, 3960–3965.
20 S. Freslon, Y. Luo, G. Calvez, C. Daiguebonne, O. Guillou, K. Bernot, V. Michel and X. Fan, *Inorg. Chem.*, 2014, **53**, 1217–1228.
21 O. Sun, T. Gao, J. Sun, G. Li, H. Li, H. Xu, C. Wang and P. Yan, *CrystEngComm*, 2014, **16**, 10460–10468.
22 N. M. Shavaleev, S. J. A. Pope, Z. R. Bell and M. D. Ward, *Dalt. Trans.*, 2003, **0**, 808–814.
23 G. Zucchi, O. Maury, P. Thuéry and M. Ephritikhine, *Inorg. Chem.*, 2008, **47**, 10398–10406.
24 W. Li, J. Li, H. Li, P. Yan, G. Hou and G. Li, *J. Lumin.*, 2014, **146**, 205–210.
25 L. Yang, Z. Gong, D. Nie, B. Lou, Z. Bian, M. Guan, C. Huang, H. J. Lee and W. P. Baik, *New J. Chem.*, 2006, **30**, 791.
26 M. Iwamuro, Y. Wada, T. Kitamura and N. Nakashima, *Phys. Chem. Chem. Phys.*, 2000, **2**, 2291–2296.
27 T. M. George, S. Varughese and M. L. P. Reddy, *RSC Adv.*, 2016, **6**, 69509–69520.
28 B. Li, H. Li, P. Chen, W. Sun, C. Wang, T. Gao and P. Yan, *Dalt. Trans.*, 2016, **45**, 11459–11470.
29 B. L. Reid, S. Stagni, J. M. Malicka, M. Cocchi, G. S. Hanan, M. I. Ogden and M. Massi, *Chem. Commun.*, 2014, **50**, 11580–11582.
30 L. Abad Galan, B. L. Reid, S. Stagni, A. N. Sobolev, B. W. Skelton, M. Cocchi, J. M. Malicka, E. Zysman-colman, E. G. Moore, M. I. Ogden and M. Massi, *Inorg. Chem.*, 2017, **56**, 8975–8985.
31 B. L. Reid, S. Stagni, J. M. Malicka, M. Cocchi, A. N. Sobolev, B. W. Skelton, E. G. Moore, G. S. Hanan, M. I. Ogden and M. Massi, *Chem. - A Eur. J.*, 2015, 1–11.
32 L. G. Van Uitert, E. F. Dearborn and J. J. Rubin, *J. Chem. Phys.*, 1967, **46**, 3551–3555.

33 T. Sano, M. Fujita, T. Fujii, Y. Hamada, K. Shibata and K. Kuroki, *Jpn. J. Appl. Phys.*, 1995, **34**, 1883–1887.
34 P. Huang, D. Chen and Y. Wang, *J. Alloys Compd.*, 2011, **509**, 3375–3381.
35 H. Zhang, Y. Wang and L. Han, *J. Appl. Phys.*, 2011, **109**, 3–8.
36 N. V. Kononets, V. V. Seminko, P. O. Maksimchuk, I. I. Bespalova, A. A. Masalov, Y. V. Malyukin and B. V. Grinyov, *Spectrosc. Lett.*, 2017, **50**, 399–403.
37 J. Bunzli and F. Ihringer, *Inorganica Chim. Acta*, 1996, **246**, 195–205.
38 W. D. W. Horrocks, M. J. Rhee, A. Peter Snyder and D. R. Sudnick, *J. Am. Chem. Soc.*, 1980, **102**, 3650–3652.
39 J. C. De Mello, H. F. Wittmann and R. H. Friend, *Adv. Mater.*, 1997, **9**, 230–232.
40 M. P. Tsvirko, S. B. Meshkova, V. Y. Venchikov, Z. M. Topilova and D. V. Bol'shoi, *Opt. Spectrosc.*, 2001, **90**, 669–673.
41 L. Abad Galan, B. L. Reid, S. Stagni, A. N. Sobolev, B. W. Skelton, E. G. Moore, G. S. Hanan, E. Zysman-Colman, M. I. Ogden and M. Massi, *Dalt. Trans*, 2018, Submitted.
42 B. L. Reid, S. Stagni, J. M. Malicka, M. Cocchi, G. S. Hanan, M. I. Ogden and M. Massi, *Chem. Commun.*, 2014, **50**, 11580–11582.
43 L. Hu, J. Zhang, Q. Yin, P. Li and K. Du, *Opt. Commun.*, 2014, **324**, 26–29.
44 S. I. Klink, G. A. Hebbink, L. Grave, P. G. B. Oude Alink, F. C. J. M. van Veggel and M. H. V. Werts, *J. Phys. Chem. A*, 2002, **106**, 3681–3689.
45 S. Omagari, T. Nakanishi, Y. Hirai, Y. Kitagawa, T. Seki, K. Fushimi, H. Ito and Y. Hasegawa, *Eur. J. Inorg. Chem.*, 2017, 1–8.
46 A. Zam, S. V Eliseeva, L. Guønøe, H. Nozary, S. Petoud and C. Piguet, *Chem. - A Eur. J.*, 2014, **20**, 12172–12182.
47 J.-C. G. Bünzli and C. Piguet, *Chem. Soc. Rev.*, 2005, **34**, 1048.